Bulletin of the Seismological Society of America, Vol. 97, No. 2, pp. 624–637, April 2007, doi: 10.1785/0120060139

Frequency-Dependent Site Amplifications with $f \geq 0.01$ Hz Evaluated from Velocity and Density Models in Central Taiwan

by Ming-Wey Huang, Jeen-Hwa Wang, Kuo-Fong Ma, Chien-Ying Wang, Jih-Hao Hung, and Kuo-Liang Wen

Abstract The frequency-dependent site amplifications at 87 free-field strong-motion station sites in central Taiwan are evaluated from the velocity and density structures constructed from borehole data measured at shallow depths and the velocity models inferred from earthquake data at great depths. Results based on the quarter-wavelength approximation method proposed by Boore and Joyner (1997) show that the site amplifications increase with frequency and are larger in the Western Plain with thick Holocene alluvium than in the Western Foothill with Pleistocene and Miocene formations. Considering wave attenuation, site amplification first increases and then decreases with increasing frequency. The turning frequency, f_t, associated with the maximum amplification varies site by site.

Introduction

Basically, four approaches can be used to evaluate the site effects from seismic data. The first approach (cf. Zhang, 2004) is a comparison between the Fourier amplitude spectra at a site and at a reference hard-rock site, with nearly flat response. However, it is not easy to locate a perfect reference site. The second approach (cf. Lermo and Chávez-García, 1993) is the calculation of horizontal-to-vertical spectral ratio at a site. The third approach (cf. Atkinson and Cassidy, 2000; Malagnini *et al.*, 2004; Sokolov *et al.*, 2004) is the ratio of the Fourier amplitude spectrum of ground motions to the spectrum simulated from a so-called "very-hard-rock model" or "absolute-source-spectra model," which is assumed to have no site effects. For the third approach, the precise source and path effects are needed. The fourth approach is the comparison between observed ground motions and values calculated on the basis of a measured velocity model assuming 1D wave propagation.

The studies of site effects in Taiwan are described in brief here. From surficial geology in Taiwan, Lee *et al.* (2001) classified 708 free-field strong-motion station sites operated by Central Weather Bureau (CWB) into three categories, that is, class C, D, and E, using a scheme compatible with the 1997 Uniform Building Code (UBC) provisions. The U.S. criteria to classify sites (Table 1) are based on shear velocities, V_s: $V_s > 1500$ m/sec for class A sites, $V_s = 760$–1500 m/sec for class B, $V_s = 360$–760 m/sec for class C, $V_s = 180$–360 m/sec for class D, and $V_s < 180$ m/sec for class E. Lee *et al.* (2001) also studied the response spectra for $f \geq 0.3$ Hz and the horizontal-to-vertical spectral ratios for $0.3 \leq f \leq 33.3$ Hz. Sokolov *et al.* (2004) established the empirical amplification functions in the frequency range 0.1–10 Hz as the ratio between Fourier amplitude spectra of recorded accelerograms and those simulated based on a hypothetical hard-rock model. Zhang (2004) evaluated the site amplification, with attenuation, for $0.7 \leq f \leq 6$ Hz. The latter two studies are both based on the site classification by Lee *et al.* (2001). As mentioned in the following the classification is not correct for numerous stations. Clearly, Sokolov *et al.* (2004) provided the model-based site effect, and others gave the reference-site-based one. Using the quarter-wavelength approximation method proposed by Boore and Joyner (1997), Huang *et al.* (2005) evaluated the site amplitudes with $f > 1$ Hz from well-logging velocity and density data measured in shallow holes near 87 of the CWB's strong-motion station sites in central Taiwan.

Although the results obtained by Huang *et al.* (2005) are significant, site amplifications only in the high-frequency regime are not enough for academic interests and engineering needs. Amplifications in a wider frequency band must be made. However, the well-logging data with depths >30 m

Table 1
The 1997 UBC Provisions for Five Classifications (cf. Lee *et al.*, 2001)

Site Classification	Provisions
A	Hard rock, eastern United States sites only, $V_s > 1500$ m/sec
B	Rock, $V_s = 760$–1500 m/sec
C	Very dense soil and soft rock, $V_s = 360$–760 m/sec
D	Stiff soils, $V_s = 180$–360 m/sec
E	Soft soils, profile with more than 10 ft (3 m) of soft clay with $V_s < 180$ m/sec

are usually not available. Hence, the velocity models inferred from earthquake data must be taken to evaluate the amplifications in the lower-frequency regime. In this study, the site amplifications at $f = 0.01 - 1$ Hz will be evaluated from the velocity and density models inferred from earthquake and microtremor data, respectively, by Chen *et al.* (2001) and Satoh *et al.* (2001). Fortunately, after the 1999 Chi-Chi earthquake the Taiwan Chelungpu-Fault Drilling Project (TCDP) was performed in 2004. Two holes with depths of about 2000 m were drilled near the northern segment of the Chelungpu fault, and the well loggings were made for V_p, V_s, ρ, etc. in the depth range 494–1866 m (Hung *et al.*, 2005). The velocity profile can be used as a constraint to examine the velocity model. In addition, the amplifications at $f \geq 1$ Hz evaluated from well-logging data of the topmost 30 m at 87 strong-motion stations by Huang *et al.* (2005) will also be described in brief.

Method

Joyner *et al.* (1981) first introduced the quarter-wavelength approximation method to evaluate the frequency-dependent site effect. In this method, the amplification at a particular frequency is the square root of the ratio of seismic impedance (velocity times density) averaged over a depth range associated with a quarter wavelength to that in the vicinity of an earthquake source. Day (1996) made some theoretical justification on the method, and stated that the amplitudes of incident waves with broad bandwidth frequency will be amplified by a factor of $2(I_b/I_0)^{0.5}$, where I_0 and I_b are shear impedance at the ground surface and basement, respectively. The approximation is insensitive to the discontinuities in seismic velocities beneath a site, and does not include nonlinear response due to the different input intensities of seismic waves.

Boore and Joyner (1997) defined the amplification to be the ratio of the Fourier amplitude spectrum of unattenuated incident-plane waves to that recorded at the surface of a uniform half-space by the same incident waves. The amplification therefore approaches unity for very-long-period waves. Boore and Joyner (1997) defined $S_{tt}(z)$ to be the average S-wave travel time, $\beta(z) = z/S_{tt}(z)$ the average velocity, $\rho(z)$ the average density, and the frequency associated with the layer thickness of z,

$$f(z) = \frac{1}{4S_{tt}(z)}. \tag{1}$$

In equation (1), $S_{tt}(z)$ is

$$S_{tt}(z) = a \cdot z^b \tag{2}$$

where a and b are trace-dependent constants. The constant a represents the surface velocity, and b is the exponent of the polynomial function of S_{tt} with z. Larger b indicates a faster increase of $S_{tt}(z)$ with z.

Amplification can be evaluated by the following equation:

$$A(f) = \sqrt{\frac{\rho_s \beta_s}{\rho(z)\beta(z)}}, \tag{3}$$

where the subscript "s" represents the source area. The five quantities are calculated from the ground surface to depth z.

In equation (3), the amplification function is evaluated only for nonattenuating waves. In fact, the site effect includes both amplification and attenuation. Anderson and Hough (1984) applied an exponential form of $e^{-\pi\kappa f}$, where κ is a frequency-independent factor, to represent attenuation at high frequencies. Campillo (1983) and Papageourgiou (1988) suggested that κ depends on the source intensity. Hanks (1982) stressed that the observed spectral amplitude decreases with increasing frequency in a higher rate when $f > f_{\max}$ than when $f < f_{\max}$. This effect will also influence the site amplification, especially at high frequencies. Hanks (1982) and Frankel (1995) stressed that $f_{\max}$ varies with site conditions. Dependence of κ on source intensity and site-specific $f_{\max}$ are beyond the scope of this study, and will not be further discussed.

Site Amplifications for $f > 1$ Hz

Project of Conducting Well-Loggings in the Upper 30 Meters

In Taiwan, a project of exploring the geological and seismic-wave velocity structures beneath strong-motion stations at both rock and soil sites has been launched by CWB and conducted by the National Center for Research on Earthquake Engineering (NCREE) since 2000. Borehole measurements of density (ρ), P-wave velocity (V_p), and S-wave (shear) velocity (V_s) were made at different depths. The density was measured directly from core samples. The velocities were measured from a Suspension P-S Logging system, which is a down-hole probe consisting of an oscillating source on the ground surface and two receivers, developed by OYO Co., Japan (Ogura, 1988). The distance between and the difference of arriving times of P or S waves recorded at the two receivers are used to measure the velocities. This method is more or less an *in situ* measurement of the velocity. The time resolution of this system is 0.001 sec, and thus, reliability of measured velocities is high. Note that in 2000, the depths of drilled holes (denoted by d_B hereafter) at a few rock sites were less than 30 m. At most sites, d_B is equal to or larger than 30 m. The values of ρ (filled circles) and V_s (a solid line) at three sites are displayed in Figure 1b. Although the velocities are measured from well shooting, for simplicity, both measured data of density and velocities are called well-logging data below. Detailed information can be found at the web site http://geo.ncree.org.tw/. In central Tai-

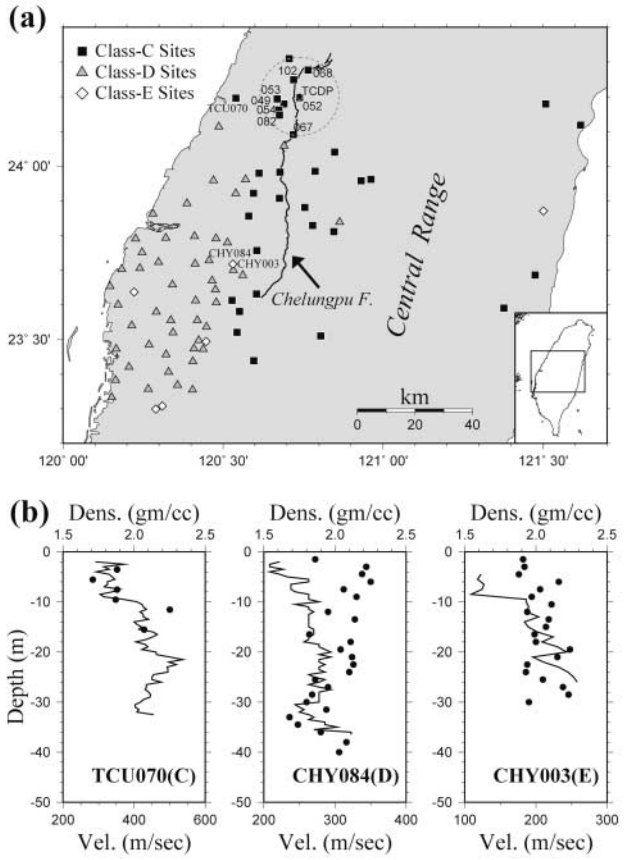

Figure 1. (a) The spatial distribution of strong-motion stations in central Taiwan (squares, triangles, and diamonds, respectively, for class C, D, and E sites). The bold-solid line displays the surface trace of the Chelungpu fault associated with the 1999 Chi-Chi earthquake. The filled circle denotes the sites of two 2000-m-deep holes of TCDP. Inside the large dashed circle, centered at the TCDP hole, with a radius of 13 km, there are eight strong-motion stations with codes. (b) The well-logging values of velocity (in a solid line) and density (in filled circles) at shallow depths at three station sites of different classes denoted by C, D, and E in the parentheses.

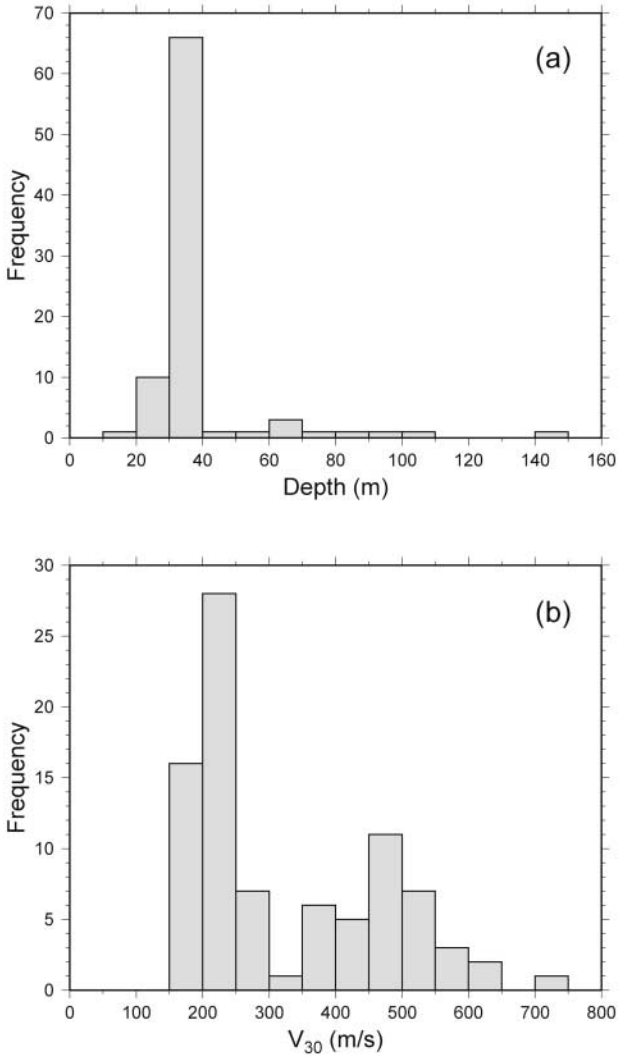

Figure 2. (a) Histogram for depths of boreholes. (b) Histogram of shear velocity averaged over the upper 30 m from well loggings (after Huang *et al.*, 2005).

wan, where the 1999 M_w 7.6 Chi-Chi earthquake was located, there are 87 boreholes, which are located in two different geological provinces, as shown in Figure 1a. Among the 87 boreholes, 82 sites are on the western part of central Taiwan, and five are in the east. There is no station in the middle of the area, which is the Central Range. Figure 2a shows the frequency distribution of depth of the 87 boreholes. The depths of 78 boreholes are less than 40 m, and the maximum depth is about 150 m.

Well-Logging Data

The shear velocities were measured at 0.5-m intervals in each hole. The total number of logging samples is 6163, and the measured shear velocity is in the range 100–900 m/sec. The density was not measured regularly at every 0.5 m and was only done at one point in a specific geological formation. The total number of logging samples is 1468 and the measured values range from 1.5 to 2.5 g/cc. Examples of logging data of *S*-wave velocity and density at three sites of different classes are displayed in Figure 1b. To construct a complete profile of density, at a hole, where only the shear velocity was measured, the density was assigned as that measured in the same geological formation at the same site or at the nearest site.

As mentioned previously, Lee *et al.* (2001) classified the 708 free-field strong-motion station sites from surficial geology based on National Earthquake Hazards Reduction Program (NEHRP) criteria (see Table 1). However, well-logging data seem to show that their classification is wrong for numerous sites. It is better to classify the site based on the directly measured values of velocity rather than the inferred ones, because the velocities of two rocks even having

the same compositions can be different due to weathering, injection of fluids, biological activities, and so on. Of course, the velocities inferred from surficial geology are still useful and significant for engineering needs when the measured ones are not available. An important site factor in influencing ground motions and in constructing the building codes (cf. Boore and Joyner, 1997) is the averaged shear velocity in the topmost 30 m, that is, $V_{30} = 30/S_{tt}(30)$. Based on NEHRP criteria for V_{30}, the classifications of 87 stations are listed in Table 2. Included also in Table 2 are the classifications by Lee *et al.* (2001). Obviously, 65 stations are reclassified. Sixty of them are upgraded and five are down-graded. Two class B stations are reclassified into class C; 1 of 6 class C stations is reclassified into class D; 24 of 38 class D stations are reclassified into class C; 2 of 38 class D stations are reclassified into class E; 1 of 39 class E stations is reclassified into class C; and 35 of 39 class E stations are reclassified into class D. Hence, there are 33 class C sites (denoted by squares), 48 class D (shown by triangles), and 6 class E (depicted by diamonds). The site conditions of the reclassified 87 stations are shown in Table 2. In western Taiwan, the class C sites are located mainly in the Western Foothill with Pleistocene and Miocene formations, and the class D and E sites are in the Western Plain with thick Holocene alluvium.

In principle, $S_{tt}(d)$ is the integral result of $z/\beta(z)$ from the ground surface to the depth d. In practice, $S_{tt}(d)$ is the sum of the values of $z/\beta(z)$ at numerous depths, separated by a small interval, for example, 0.5 m in this study. Because $d_B < 30$ m for a few holes, the calculations of S_{tt} are different between $d_B < 30$ m and $d_B \geq 30$ m. When $d_B \geq 30$ m, $S_{tt}(30)$ is the sum of $0.5/\beta(z)$ in the topmost 30 m. When $d_B < 30$ m, the value of $S_{tt}(d_B)$, which is the sum of $0.5/\beta(z)$ within d_B, is extrapolated to $S_{tt}(30)$ by using a power-law function as explained in the following. Figure 2b displays the frequency distribution of V_{30}. The values of V_{30} are in the range 200–700 m/sec. The formations of core samples belong to three geological periods, that is, the Holocene, Pliocene, and Miocene; and the major geological materials are the clays of high plasticity, silty soils, silty sand, sand-silt mixture, etc. In Figure 2b, there are two groups with different peaks: the first one with a peak at about 450 m/sec for class C sites and the other with a peak near 250 m/sec for class D and E sites. The distribution is more dispersed for class C sites than for class D and E sites.

Table 2
Classifications of 87 Station Sites Based on V_{30} Criteria (the Site Classifications made by Lee *et al.* [2001] are Shown in Parentheses)

Station	Class	Station	Class	Station	Class
CHY001	D (E)	CHY002	D (E)	CHY003	E (D)
CHY004	D (E)	CHY005	D (E)	CHY006	C (D)
CHY007	D (E)	CHY008	D (E)	CHY009	D (D)
CHY012	D (E)	CHY013	D (E)	CHY015	D (D)
CHY024	C (D)	CHY025	D (E)	CHY026	D (E)
CHY027	D (E)	CHY028	C (D)	CHY029	C (C)
CHY030	D (D)	CHY031	D (E)	CHY032	D (E)
CHY033	D (E)	CHY034	C (D)	CHY036	D (D)
CHY037	D (D)	CHY038	D (C)	CHY039	D (E)
CHY041	C (D)	CHY043	D (E)	CHY044	D (E)
CHY047	E (D)	CHY048	D (D)	CHY049	D (E)
CHY054	E (E)	CHY073	D (D)	CHY074	C (C)
CHY076	E (E)	CHY082	D (E)	CHY084	D (E)
CHY092	D (E)	CHY093	D (E)	CHY094	D (E)
CHY095	D (E)	CHY101	D (D)	CHY103	D (D)
CHY104	D (E)	CHY105	D (E)	CHY106	D (D)
CHY107	E (E)	CHY111	D (E)	CHY112	D (E)
CHY113	D (E)	HWA026	C (B)	HWA033	C (C)
HWA034	C (D)	HWA056	C (B)	HWA059	E
TCU049	C (D)	TCU052	C (D)	TCU053	C (D)
TCU054	C (D)	TCU065	D (D)	TCU067	C (D)
TCU068	C (D)	TCU070	C (C)	TCU071	C (D)
TCU072	C (D)	TCU074	C (D)	TCU075	C (D)
TCU076	C (D)	TCU077	C (D)	TCU078	C (D)
TCU079	D (D)	TCU082	C (D)	TCU086	D (E)
TCU102	C (D)	TCU103	C (D)	TCU110	D (E)
TCU111	D (E)	TCU113	D (E)	TCU115	D (E)
TCU116	C (E)	TCU120	C (C)	TCU138	C (D)
TCU139	D (E)	TCU143	C (D)	TCU148	C

Evaluation of Site Amplifications from Well-Logging Data

To evaluate the depth functions of amplifications, it is necessary first to construct $S_{tt}(z)$ based on equation (2). Taking the common logarithms of equation (2) leads to:

$$\log[S_{tt}(z)] = a' + b \times \log(z), \tag{4}$$

where $a' = \log(a)$. The constants a' and b can be evaluated by using the least-squares method. The resultant equations with a correlation coefficient denoted by σ are: $\log(S_{tt}) = (1.64 \pm 1.01) + (0.87 \pm 0.01) \times \log(z)$ with $\sigma = 0.99$ for station TCU070; $\log(S_{tt}) = (2.96 \pm 1.01) + (0.92 \pm 0.01) \times \log(z)$ with $\sigma = 0.99$ for station CHY084; and $\log(S_{tt}) = (2.84 \pm 1.06) + (0.79 \pm 0.01) \times \log(z)$ with $\sigma = 0.99$ for station CHY003. Large σ shows a high correlation between the two quantities. For each class of site, the plot of S_{tt} versus z (in filled circles) and the linear-regression equation (in a solid line) are displayed in Figure 3. Displayed also in Figure 3 are the dashed lines representing the standard deviations. Obviously, the linear-regression line fits the data very well. For all station sites, the plots of $S_{tt}(z)$ versus z are depicted in Figure 4. Obviously, $S_{tt}(z)$ can be divided into three groups, each associated with a class of sites, which are shown with different kinds of symbols: squares for class C sites, triangles for class D sites, and diamonds for class E sites. The regression-power functions of $S_{tt}(z)$ versus z are depicted in Figure 4 by the dashed lines, which fit the data points very well. To calculate V_{30}, extrapolation must be made for estimating the value of $S_{tt}(z)$ at $z = 30$ m from the least-squares fit at the holes with $d_B < 30$ m.

Two holes with depths of 455 and 211 m, respectively,

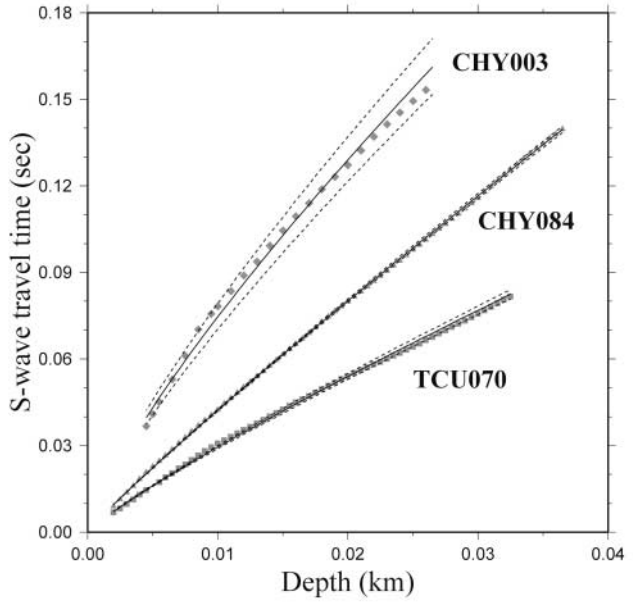

Figure 3. The plots of S_{tt} versus z at three station sites: TCU070 (class C), CHY084 (class D), and CHY003 (class E). The solid and dashed lines denote the linear-regression equations and the standard errors, respectively.

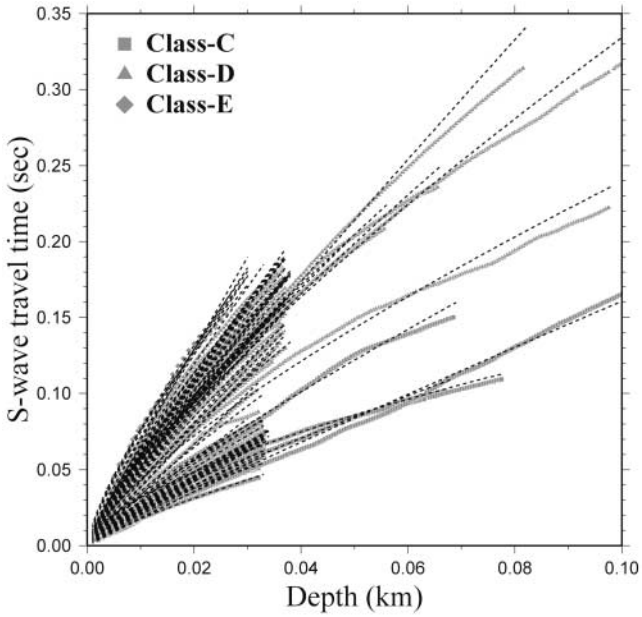

Figure 4. S_{tt} versus depth: squares, triangles, and diamonds are data points for class C, D, and E sites, respectively. The least-squares fit of a power-law function is depicted by a dashed line (after Huang *et al.*, 2005).

were drilled near the Chelungpu fault (see Fig. 1a) (Tanaka *et al.*, 2002). The densities measured from the loggings increase gradually with depth, reaching a value of about 2.8 g/cc, which is taken to be ρ_s. From Ma *et al.* (1996), the average crustal shear velocity, that is, 3500 m/sec, is taken to be β_s.

Evaluations of site amplifications are described in the following. First, from the measured values of $\beta(z)$ and $\rho(z)$ we calculate $A(f)$ and $f(z)$ at a single borehole. Results are displayed in Figure 5 with different open symbols: squares, triangles, and diamonds, respectively, for class C, D, and E sites. Second, average $A(f)$ for a class of sites is calculated from the values of $A(f)$ at all holes of the class at the same depth. The values at several frequencies in between 1 and 39.6 Hz for the three classes of sites are given in Table 3. The numbers of logging data for class E sites are small. At lower frequencies, the numbers for class C and D sites are also small. The data points of average $A(f)$ versus average $f(z)$ are displayed in Figure 5 with filled symbols, squares, triangles, and diamonds, respectively, for class C, D, and E sites. Included also in Figure 5 are the error bars for both $A(f)$ and $f(z)$. Essentially, $A(f)$ increases with $f(z)$ for the three classes of sites. The values of average $A(f)$ approach 3.8, 5.5, and 6.1, respectively, for class C, D, and E sites when $f(z) > 10$ Hz.

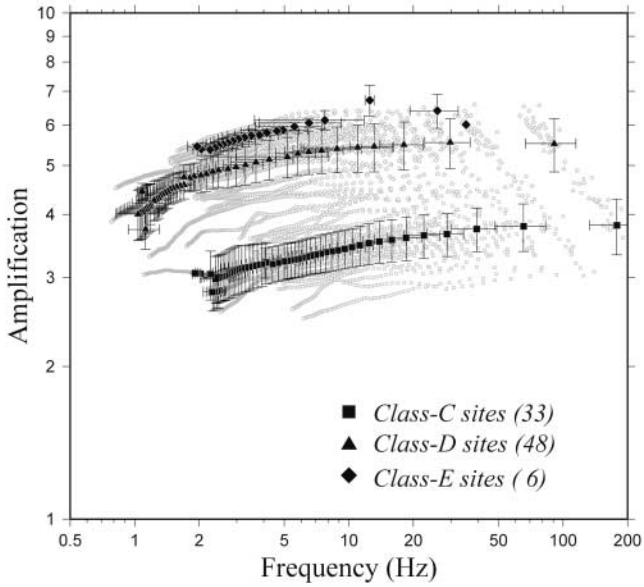

Figure 5. The plots of $A(f)$ versus f: open squares, open triangles, and open diamonds for class C, D, and E sites, respectively. The average values, with error bars, for the three classes of sites are displayed by the respective filled symbols (after Huang *et al.*, 2005).

The frequency ranges are different for the three classes of sites. The parameter $V_{30} = 30/S_{tt}(30)$ (in meters per second) controls the magnitude of lower-bound frequency, f_{low}, associated with the topmost 30 m. The calculated values of V_{30} are 383.9–709.0, 185.8–359.1, and 158.3–175.0 m/sec for class C, D, and E sites, respectively. The values of related f_{low} are 3.0–5.9, 1.5–3.0, and 1.3–1.5 Hz for class C, D, and E sites, respectively. In Figure 5, for class C sites, except for few boreholes with $d_B > 30$ m, there are no data points for $f(z) < 2$ Hz. The plots can be divided into three groups,

Table 3
The Values of Site Amplifications, $A(f)$, for Class C, D, and E Sites Evaluated Based on Well-Logging Data

Frequency (Hz)	Classification		
	C	D	E
1.0		4.5 (3)	
2.3	2.8 (2)	4.9 (45)	5.4 (3)
3.1	3.1 (4)	5.0 (48)	5.6 (4)
5.0	3.2 (32)	5.2 (48)	6.9 (5)
11.0			6.2 (5)
25.8			6.4 (3)
28.8	3.7 (31)		
29.7		5.6 (46)	
39.6	3.7 (32)		

The number of boreholes at the same depth used in estimating the $A(f)$ is given in parentheses.

associated with class C, D, and E sites, respectively, from top to bottom. The plots of class D and E sites are close to each other.

Site Amplifications for 20 Hz $> f >$ 0.01 Hz

Velocity Models Inferred from Earthquake Data

The shallow boreholes cannot provide well-logging data for evaluations of site amplifications when $f < 1$ Hz. Although there are a few holes with depths greater than 100 m in central Taiwan, the data are either incomplete or not available. An alternative way to construct the deeper velocity models from seismic studies must be taken into account. Chen *et al.* (2001) used a large earthquake data set to infer the 3D velocity model in central Taiwan. Their result shows a variation in the *S*-wave velocities in different depth intervals: 0–2 km, 2–5 km, 5–10 km, 10–15 km, 15–25 km, and 25–35 km. They stated that the velocities in the first four shallower depth intervals have the better resolutions and less uncertainty due to the comprehensive ray paths passing through. According to Boore and Joyner (1997), $A(f)$ is approximately unity when $f \leq 0.01$ Hz, corresponding to a depth of deeper than about 10 km. Hence, the velocities in the depth interval of 2–10 km are important on evaluations of site amplifications at lower frequencies.

Satoh *et al.* (2001) investigated the *S*-wave velocity structure of the Taichung Basin from microtremors detected by a local, temporary array, which is almost collocated with strong-motion stations. They inferred the thickness of a layer with a particular velocity, such as $V_s = 116$, 278, 657, and 1100 m/sec, by using the method of horizontal-to-vertical spectral ratios (HVRs). Results show that the layer with $V_s =$ 1100 m/sec has a thickness of about 1000–1400 m in the east-central part of Taichung basin. At 10 stations, that is, TCU049, TCU052, TCU053, TCU054, TCU065, TCU67, TCU068, TCU070, TCU082, and TCU102, where the velocity models were inferred by Satoh *et al.* (2001), the well loggings were also conducted.

To construct a velocity model, we take differentiation of equation (2) about z. This leads to

$$\frac{\partial S_{tt}(z)}{\partial z} = a \cdot b \cdot z^{b-1} \tag{5}$$

By taking the inverse of equation (5), we obtain

$$\beta(z) = \frac{\partial z}{\partial S_{tt}(z)} = c \cdot z^{d} \tag{6}$$

where $c = /(a \cdot b)$, $d = 1 - b$, and $\beta(z)$ is the representative velocity at depth z. From equation (6), the velocity can be represented as a power-law function of z. Equation (6) requests a monotonic increase in velocity with depth, and, thus, a low-velocity layer is averaged out during the regression procedure. This would underestimate amplifications at some frequencies associated with the low-velocity layer and is a significant problem to resolve.

Velocity Models

Before constructing a velocity model as a form of equation (6), the vertical velocity structure is divided into three depth ranges with different constants c and d: the shallow range (0, d_B km), the middle one (d_B, 2 km), and the deep one (2–8 km). For example, Figure 6 shows the depth distribution of *S*-wave velocity beneath station TCU052. Well-logging data are shown by a dotted line, while the velocities inferred by Chen *et al.* (2001) and Satoh *et al.* (2001) are represented by a dashed line. Using least-squares fitting, the c and d in equation (6) can be inferred and the resultant velocity-depth functions are plotted in Figure 6 with a solid line. The velocity models for the 86 sites are constructed in this way. As shown in Figure 6, the values of c and d for the shallow depths from well-logging velocities are different from those at depths from inferred velocities. Therefore, for each station site three pairs of c and d are evaluated for the previously mentioned depth ranges.

As mentioned previously, two holes with depths of about 2000 m were drilled near the northern segment of the Chelungpu fault, and the well loggings were made for measuring V_p, V_s, ρ, etc. in the depth range 494–1866 m (Hung *et al.*, 2005). In Figure 1a, a filled circle denotes the location of two TCDP's deep holes. Inside a large dashed circle, with a radius 13 km, centered at the TCDP's deep hole, there are eight strong-motion stations, that is, TCU049, TCU052, TCU053, TCU054, TCU067, TCU068, TCU082, and TCU102. We compare the depth distributions of *S*-wave velocities of the two TCDP deep holes in the depth range 494–1866 m (displayed in Fig. 7 with a gray line) and those of the velocities inferred by Chen *et al.* (2001) and Satoh *et al.* (2001). It is obvious that in the depth range 494–800 the velocity increases linearly with depth, with an average of 1.65 km/sec, whereas in the depth range 800–1866 m the velocity varies around an average of 1.93 km/sec. Also in-

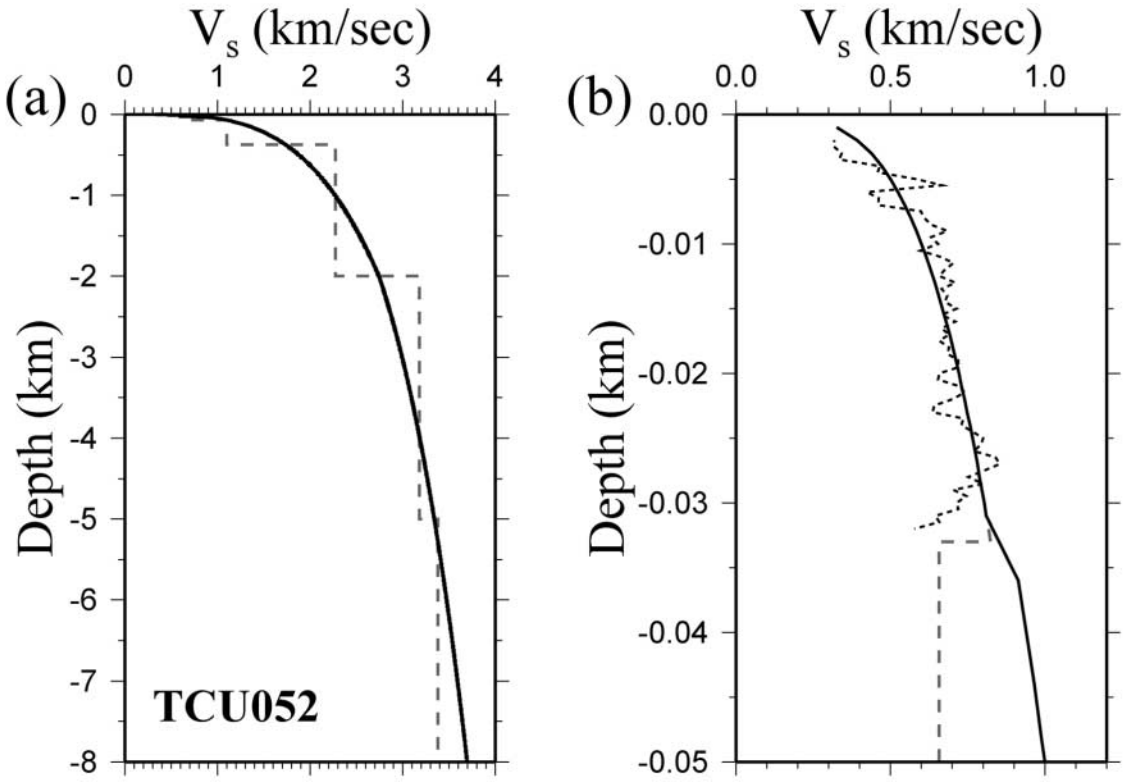

Figure 6. An example to show the depth distribution of *S*-wave velocity beneath station TCU052: (a) for 0 to −8 km and (b) for 0 to −0.05 km. The dotted line denotes the well-logging velocities, $V_s(z)$, and the dashed line displays the velocity model inferred by Chen *et al.* (2001) and Satoh *et al.* (2001). The solid line represents the best fit of the velocity-depth function based on equation (6).

cluded in Figure 7 displayed with the gray lines are the well-logging velocities in the topmost 30 m. The dashed lines represent the velocities inferred by Chen *et al.* (2001) and Satoh *et al.* (2001), and the solid lines denote the exponential velocity-depth functions evaluated from equation (6). The dotted lines show the new exponential velocity-depth functions estimated from well-logging data using equation (6). Due to the limitations of well-logging data, the new velocity-depth functions are plotted downward only to a depth of 2000 m through extrapolation. Except for station TCU067, the well-logging velocities are about 0.3 km/sec smaller than the inferred ones. At station TCU067, the average well-logging velocity is about 0.73 km/sec larger than the inferred one. Among the eight stations, this station is to the south of and has the largest distance to the deep-hole site. However, the difference is small. For the eight stations, the difference between the solid and dotted lines, which are made through regression based on equation (6), increases with depth. This is because the solid line is inferred from a velocity model including higher velocities at depths, while the well loggings were made only in the depth range 494–1866 m. Clearly, results suggest that the inferred velocity model can be accepted to evaluate the site amplifications.

Density Models

The density model is also necessary for evaluating the site amplifications. Boore and Joyner (1997) provided an empirical relationship between ρ and β in North America by the following equation:

$$\rho = 2.5 + (\beta - 0.3) \times \frac{2.8 - 2.5}{3.5 - 0.3} \qquad (7)$$

Klimis *et al.* (1999) proposed two simple linear functions of ρ versus β for class C and D sites in Greece. For the class C sites, the function is

$$\rho = 2.0 + (\beta - 0.25) \times \frac{2.7 - 2.0}{3.4 - 0.25}. \qquad (8)$$

For class D sites, the function is

$$\rho = 1.9 + (\beta - 0.16) \times \frac{2.7 - 1.9}{3.4 - 0.16}. \qquad (9)$$

In equations (7)–(9), the density and velocity are, respectively in a unit of g/cm^3 and km/sec.

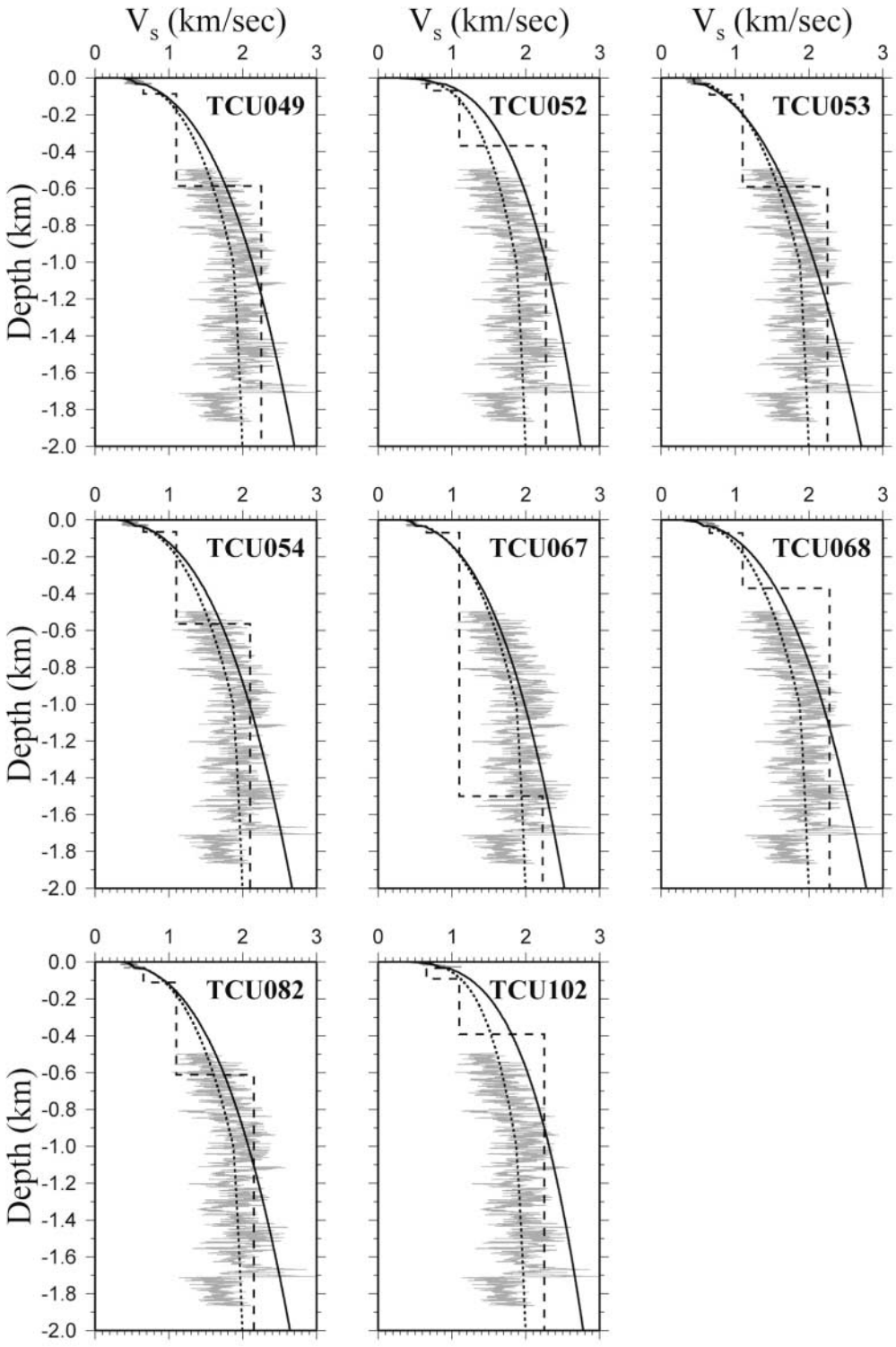

Figure 7. The depth distributions versus V_s below the eight stations inside the large dashed circle shown in Figure 1a. The gray and dashed lines represent, respectively, well-logging velocity models inferred from earthquake data by Chen *et al.* (2001) and Satoh *et al.* (2001). The solid and dotted lines are the velocity-depth functions inferred, respectively, from well-logging and modeled velocity based on equation (6).

Boore and Joyner (1997) and Klimis *et al.* (1999) both suggested that the relation of density versus *S*-wave velocity can be obtained through linear interpolation of the values of the two parameters measured at two ends of a hole. However, this way is not accessible in central Taiwan, because of a lack of such data. From well-logging data, the density is about 2.0 g/cm^3 with respect to the *S*-wave velocity of 0.3 km/sec from well-logging data. Incorporating the parameters, that is, ρ_s and β_s, of the source area, we propose an empirical function between density and *S*-wave velocity in the study area:

$$\rho = 2.0 + (\beta - 0.3) \times \frac{2.8 - 2.0}{3.5 - 0.3}. \qquad (10)$$

Obviously, the differences among equation (7) for North America, equations (8) and (9) for Greece, and equation (10) for central Taiwan are small. The depth variation in density is much smaller than that of velocity. Therefore, the dominant role on the amplification functions is the velocity.

Results

Examination of Reliability

For comparison, the amplification functions at eight stations, which are located inside a large dashed circle in Figure 1a, are evaluated from two velocity models. The first velocity model consists of the well-logging velocities at shallow depths and the inferred velocities at great depths, and is called VM1. The second velocity model, in which the well-logging velocities in the depth range 494–1866 m are incorporated with VM1, is named VM2. The density in use is calculated from the *S*-wave velocity from equation (10). Results are shown in Figure 8, where the amplification functions evaluated from VM1 and VM2 are depicted, respectively, by the solid and dashed lines. The frequencies associated with the borehole depths from 494 to 1866 m are 3–0.2 Hz. Figure 8 shows that the two lines are very close when $f > 1$ Hz, yet depart when $f < 1$ Hz. Although the differences can be up to 22% (between 1.35 and 1.62) and 20% (between 1.32 and 1.59) at $f = 0.2$ Hz for stations TCU052 and TCU102, respectively, the difference, in general, is small. Therefore, it can be assumed that the amplification functions evaluated from the velocity models inferred from earthquake data are acceptable.

Amplification Functions Evaluated from the Velocity and Density Models

Based on the velocity and density models underneath the 87 sites, the frequency-dependent site amplifications are constructed by using the method described previously. The amplifications in the frequency range 0.01–20 Hz for class C, D, and E sites are plotted in Figure 9. Note that the signals with $f > 20$ Hz are less useful for engineering needs and, thus, only the amplifications for $f \leq 20$ Hz are shown in Figure 9. Included in Figure 9 are average amplifications and the standard deviations: open squares, open triangles, and open diamonds, respectively, for class C, D, and E sites. The maximum values of average amplifications are 3.6, 5.5, and 6.7, respectively, for class C, D, and E sites in Taiwan. The standard deviation is obviously large when $f > 1$ Hz, because of the large variety in velocities at shallow depths as shown in Figure 4. Figure 9 shows that for all sites, the amplification is 1 at $f = 0.01$ and increases gradually with frequency. The evaluated values of site amplifications, $A(f)$, at some frequencies in the range 0.01–21 Hz for class C, D, and E sites are listed in Table 4.

Corrections due to Attenuation

For attenuation in the form of $e^{-\pi\kappa f}$, Sokolov *et al.* (2004) took $\kappa = 0.03 - 0.05$ sec for earthquakes with magnitudes of 5–7.6. Here, three values, that is, 0.03, 0.04, and 0.05 sec, are taken to correct the average amplifications for class C and D sites. Results are shown in Figure 10 (with the solid lines). Unlike the original function, the corrected amplifications first increase and then decrease with increasing frequency. A turning frequency, f_t, is associated with the peak amplification.

Discussion

Figure 4 shows that $S_{tt}(z)$ in the topmost several ten meters increases with depth almost in a power-law form, that is, $S_{tt}(z) \sim z^n$, which is depicted by a dashed line in Figure 4. The n varies site by site, with the largest n at a class E site, the middle n at a class D site, and the smallest n at a class C site.

Figure 5 shows that the amplification-frequency functions, evaluated from the shallow velocity and density models, of the three classes of sites all increase with frequency. However, the functions become flat when $f > 10$ Hz. The amplification functions reflect the effects due to velocity structures: $z > 30$ m for $f < 1$ Hz and $z < 30$ m for $f > 1$ Hz. Thus, flatness implies uniform velocity structure at shallow depths. The amplifications at class D sites are about 1.7 times larger than those at class C ones. The amplifications at class E sites are about 1.2 times larger than those at class D ones. As mentioned previously, almost all class C sites are located at the Western Foothill with Pleistocene and Miocene formations, and the class D and E sites in the Western Plain with thick Holocene alluvium. The shear velocities and densities are higher at class C sites than at class D and E sites, thus leading to smaller amplifications at the former than at the latter two. Note that a correlation between site amplification and local geology cannot be delineated currently, because of complex core samples.

Figure 9 shows the frequency-dependent amplification functions and the average ones, evaluated from the velocity and density models with depths less than 8 km, of the three

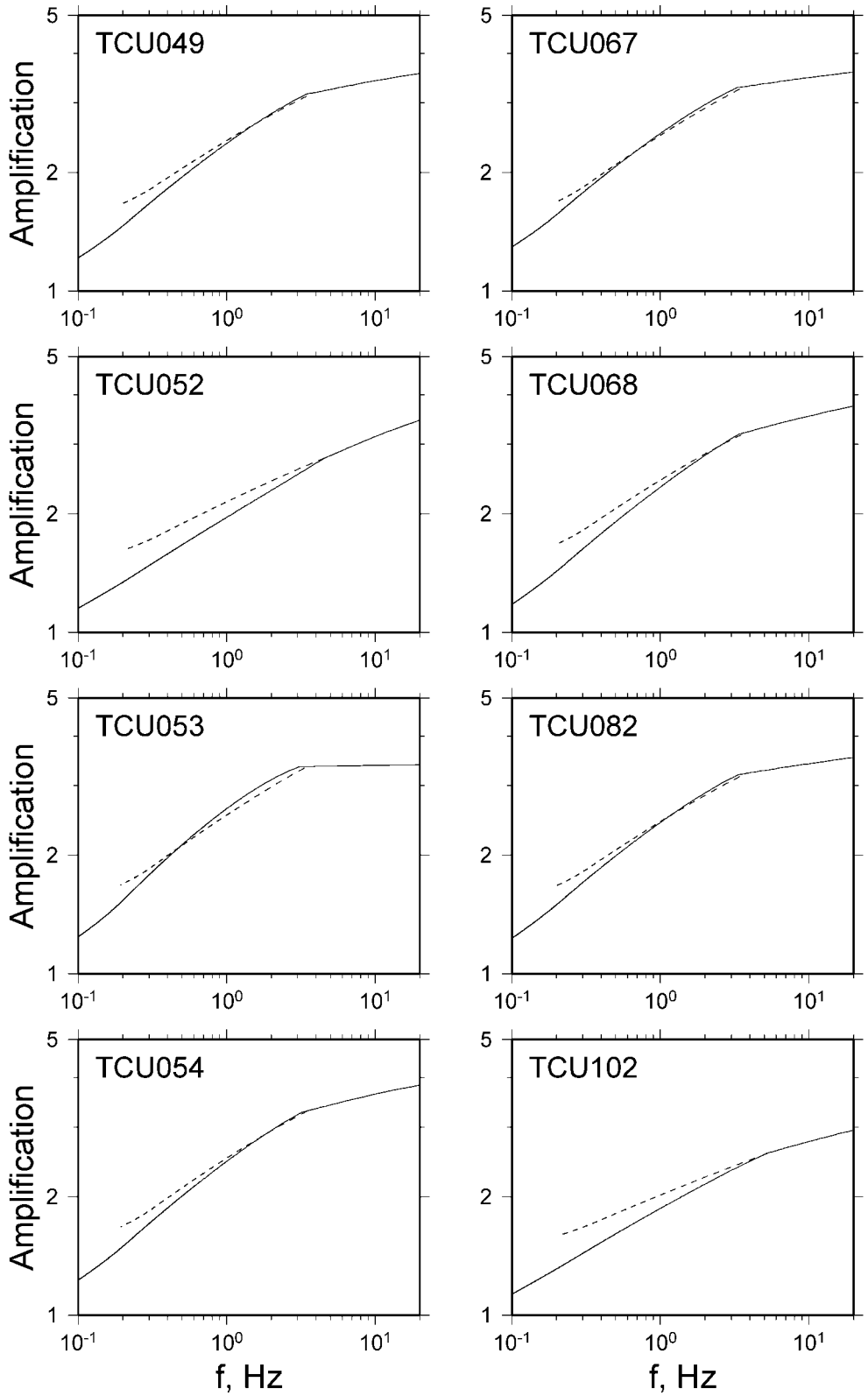

Figure 8. The plots of amplification versus frequency for the eight stations inside the large dashed circle shown in Figure 1a. The solid and dashed lines represent the amplification functions evaluated from the velocity-depth functions inferred, respectively, from the well-logging and modeled velocities as shown in Figure 7.

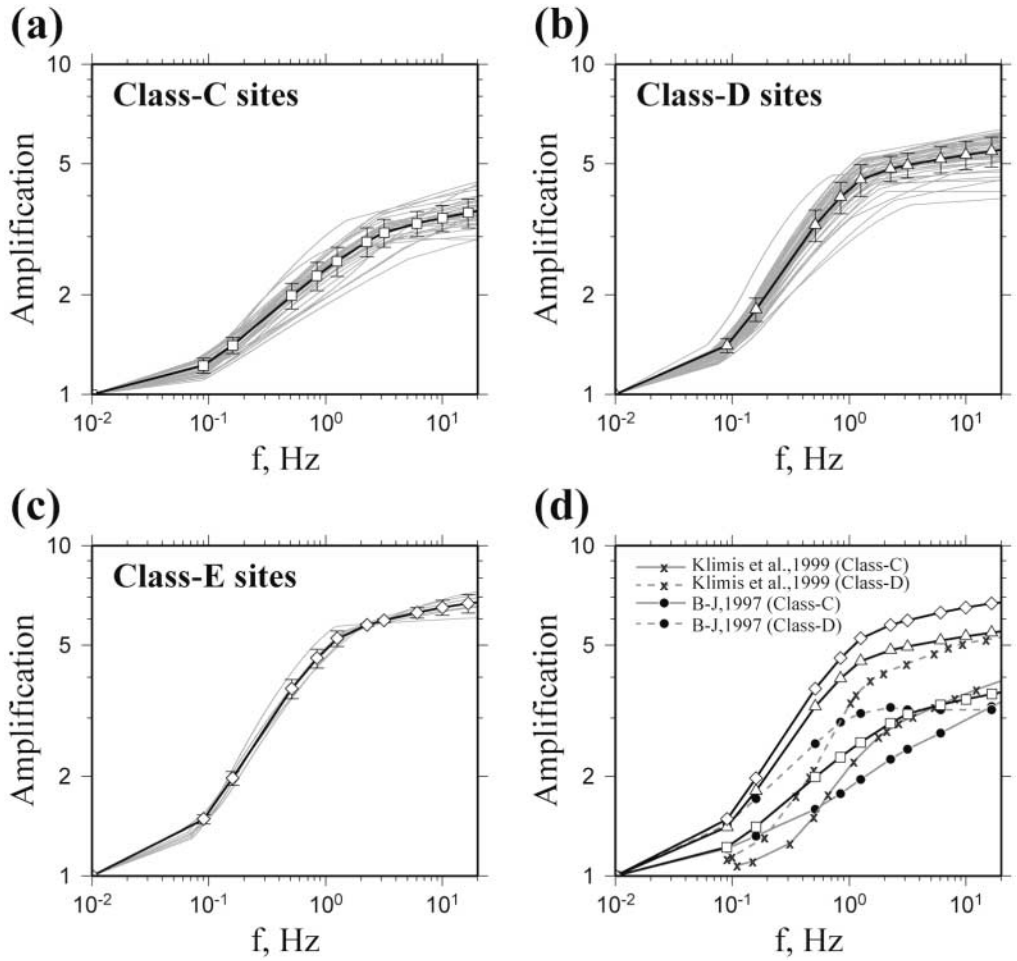

Figure 9. The plots of amplification versus frequency: open squares, open triangles, and open diamonds, respectively, for class C, D, and E sites. The average amplifications for the three classes of sites are displayed in the left, bottom diagram. Included also in this diagram are the amplification-frequency functions in North America (lines with crosses) and Greece (lines with circles) evaluated, respectively, by Boore and Joyner (B-J) (1997) and Klimis *et al.* (1999): the solid and dashed lines, respectively, for class C and D sites.

classes of sites in the frequency range 0.01–20 Hz. Obviously, the amplifications all increase with frequency. However, the functions become flat when $f > 10$ Hz. The increasing rate is larger at $f = 0.1$–1 Hz than at other frequencies. This might be due to great variety in velocities in the depth range 30–2000 m. Site amplifications are largest at class E sites, intermediate at class D, and smallest at class C.

Included also in Figure 9d are the amplification functions of Greece (lines with crosses) evaluated by Klimis *et al.* (1999) and those of North America (lines with circles) done by Boore and Joyner (1997): solid lines for class C sites and dashed lines for class D sites. For class C sites, the amplifications of Greece are lower or higher than ours when $f < 5$ Hz or when $f > 5$ Hz; and those of North America are lower than ours are when $f < 30$ Hz. For class D sites, the amplifications of both Greece and North America are smaller than ours in the frequency range 0.01–20 Hz. In addition, for both class C and D sites the amplifications of North America and this study are almost matched when $f <$ 0.1 Hz. This indicates that the velocity models of the two regions at great depths are almost the same. For class D sites the difference in amplifications between Greece and this study is small when $f > 10$ Hz. This indicates that the velocity models of Greece and the Western Plain in central Taiwan at shallow depths are almost the same.

Figure 10 shows the effect on the site amplifications caused by high-cut filtration with a form of $e^{-\pi\kappa f}$. Obviously, the corrected amplitude first increases and then decreases with increasing frequency. The turning frequency, f_t, associated with the peak amplification slightly increases with κ for class C sites and is almost constant for class D sites. Its

Table 4
The Values of Site Amplifications, $A(f)$, in the Frequency Range 0.01–21 Hz for Class C, D, and E Sites Evaluated from the Velocity Structures Constructed from Well-Logging Data and Velocity Models Inferred from Earthquake Data in Central Taiwan

Frequency (Hz)	Classification		
	C	D	E
0.01	1.00	1.00	1.00
0.09	1.22	1.41	1.48
0.16	1.41	1.81	1.97
0.51	1.99	3.25	3.68
0.84	2.29	3.96	4.56
1.25	2.53	4.47	5.23
2.26	2.90	4.83	5.75
3.17	3.09	4.95	5.93
6.05	3.29	5.16	6.26
10.0	3.43	5.32	6.49
16.6	3.55	5.45	6.67
21.0	3.61	5.50	6.75

values are larger at class C sites than at class D sites. For both class C and D sites, the difference on the amplifications between any two values of κ is almost zero when $f < 0.5$ Hz and increases with frequency when $f > 0.5$ Hz.

Sokolov *et al.* (2004) evaluated the amplifications at $f =$ 0.1–10 Hz across the entire Taiwan region. They defined the site amplification to be the ratio of the observed Fourier spectrum to the model spectrum calculated from $A(f) = (2\pi f)^2 CS(f)D(r, f)I(f)$, where C is the scaling factor, $S(f)$ is the source spectrum, $D(r, f)$ is the attenuation function, $I(f)$ is the instrumental response, and r is the hypocentral distance. $D(r, f)$ is $e^{-\pi f r/\beta Q(f)} \cdot e^{-\kappa \pi f}$, where $Q(f)$ is the quality factor and $e^{-\kappa \pi f}$ represents wave attenuation. They used $Q(f) = 80f^{0.8}$ obtained by Sokolov *et al.* (2004) for the shallow crustal structures and took $\kappa = 0.03$ sec. Their studies were based on the site classification by Lee *et al.* (2001). They only evaluated amplifications for $f > 0.3$ Hz. Results are displayed in Figure 10 with a dashed line. For class C sites, their values are larger than those of this study in two frequency ranges, 0.1–0.45 Hz and 1.9–6.5 Hz, yet smaller than those of this study in two frequency ranges, that is, 0.45–1.9 Hz and 0.5–11 Hz. In general, the dashed line is comparable to the solid line with $\kappa = 0.03$ sec. This indicates that $\kappa = 0.03$ sec is appropriate for class C sites. Although the frequency-dependent amplifications obtained by Sokolov *et al.* (2004) are the averages for the entire Taiwan region, the results can be applied to class C sites, which are on rock or thin alluvium in the Western Foothill. Meanwhile, the relationship of $Q = 80f^{0.8}$ seems able to represent seismic-wave attenuation for the Western Foothill in the study area.

On the other hand, the values for class D sites by Sokolov *et al.* (2004) are smaller than those of this study for the three values of κ. Except for the frequency range 0.3–2.0 Hz, the dashed line is obviously close to the solid line with $\kappa = 0.05$ sec, yet below the others. This indicates that $\kappa = 0.05$ sec is appropriate for class D sites. Why must a larger value of κ be used for the class D sites? There are two reasons to cause low amplifications at class D sites obtained by Sokolov *et al.* (2004). First, their very-hard-rock model might not be completely appropriate for the Western Plains in the study area. Second the relationship $Q = 80f^{0.8}$, which is an average for the entire Taiwan region, is not suitable for the study area, which is in the Western Plains covered by thick Holocene alluvium with a few kilometers in thickness. The sedimentary layers are usually specified with low Q. In the Western Plain, the Q-value is not available, and,

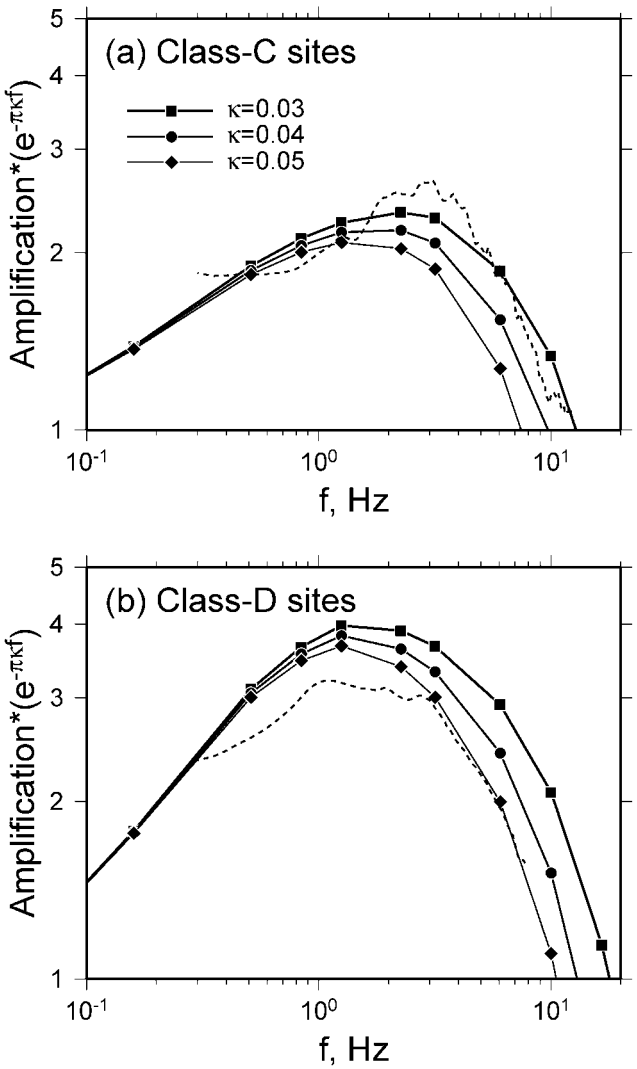

Figure 10. The plots of average amplification (corrected by high-cut filtration) versus frequency for class C and D sites with three values of κ, that is, 0.03 sec (in solid squares), 0.04 sec (in solid circles), and 0.05 sec (in solid diamonds). The dashed lines display the site amplifications obtained by Sokolov *et al.* (2004).

thus, a direct calculation to examine the effect is impossible. Nevertheless, the Q-value in the Ilan plain in northeast Taiwan can help us to understand the problem. Shieh (1992) reported $Q < 30$, with two exceptions of 44.4 and 50.7, for the sedimentary layers below the plain. The sedimentary layers are much thicker in the Western Plain than in the Ilan Plain. The thickness of the former is a few kilometers and can be up to 5 km (cf. Ma *et al.*, 1996), and that of the latter is merely between 100 and 400 m (Jiang, 1976). Hence, low Q must be taken to correct the amplifications evaluated by Sokolov *et al.* (2004) in the Western Plain. As shown in Figure 10, for class D sites the solid line with $\kappa = 0.05$ sec is more appropriate to describe the dashed line than that with $\kappa = 0.03$ sec. This seems to compensate for the use of a higher Q for the thick sedimentary layers in their study. Therefore, we conclude that $\kappa = 0.05$ sec must be used for class D sites to describe high-frequency wave attenuation rather than $\kappa = 0.03$ sec.

Conclusions

As shown in Table 2, 65 stations are reclassified based on the values of V_{30} evaluated from well-logging velocities at shallow depths. Sixty of them are upgraded and five downgraded.

From the quarter-wavelength approximation method by Boore and Joyner (1997), we evaluate the frequency-dependent site amplifications at 87 free-field strong-motion stations in central Taiwan from the velocity and density structures constructed from two origins: well-logging data measured in shallow holes near station sites and the average velocity models for the area inferred from earthquake data by Chen *et al.* (2001) and Satoh *et al.* (2001). Well-logging velocities measured at shallow and deep holes suggest reliability of the velocities, at least in the upper 2000 m, inferred by earthquake data. Results show two key points: (1) The site amplifications are the largest at class E sites, intermediate at class D, and smallest at class C; and (2) before considering wave attenuation, the site amplification increases with frequency for all classes. Together with regional geology, the first point leads to site amplification being larger in the Western Plain with thick Holocene alluvium than in the Western Foothill with Pleistocene and Miocene formations.

For class C sites, the amplifications of Greece are slightly lower than ours are when $f < 5$ Hz and larger than ours are when $f > 5$ Hz; and those of North America are lower than ours are when $f < 30$ Hz. For class D sites, the amplifications of both Greece and North America are smaller than ours in the frequency range 0.01–30 Hz. The velocity models of North America and central Taiwan at great depth are almost the same, whereas the velocity models of Greece and the Western Plain in central Taiwan at shallow depths are similar.

Comparison between the amplification functions obtained by Sokolov *et al.* (2004) and those of this study shows that $\kappa = 0.03$ sec and 0.05 sec are appropriate, respectively, for class C and D sites.

Acknowledgments

We thank M. Chapman (Associate Editor), T. Satoh, and an anonymous reviewer for numerous valuable comments and suggestions. This study was financially supported by Academia Sinica and the National Sciences Council under grant no. NSC94-2119-M-001-011.

References

Anderson, J., and S. Hough (1984). A model for the shape of the Fourier amplitude spectrum of acceleration at high frequencies, *Bull. Seism. Soc. Am.* **74,** 1969–1993.

Atkinson, G. M., and J. F. Cassidy (2000). Integrated use of seismograph and strong-motion data to determine soil amplification: response of the Fraser River Delta to the Duvall and Georgia Strait earthquake, *Bull. Seism. Soc. Am.* **90,** 1028–1040.

Boore, D. M., and W. B. Joyner (1997). Site amplifications for generic rock sites, *Bull. Seism. Soc. Am.* **87,** 327–341.

Campillo, M. (1983). Numerical evaluation of near-field, high-frequency radiation from quasi-dynamic circular faults, *Bull. Seism. Soc. Am.* **73,** no. 3, 723–734.

Chen, C.-H., W.-H. Wang, and T.-L. Teng (2001). 3D velocity structures around the source area of the 1999 Chi-Chi, Taiwan, earthquake: Before and after the mainshock, *Bull. Seism. Soc. Am.* **91,** no. 5, 1013–1027.

Day, S. M. (1996). RMS response of a one-dimensional half space to SH, *Bull. Seism. Soc. Am.* **86,** 363–370.

Frankel, A. (1995). Simulating strong motions of large earthquakes using recordings of small earthquakes: the Loma Prieta mainshock as a test case, *Bull. Seism. Soc. Am.* **85,** no. 4, 1144–1160.

Hanks, T. (1982). f_{max}, *Bull. Seism. Soc. Am.* **72,** 1867–1879.

Huang, M.-W., J.-H. Wang, H.-H. Hsieh, K.-L. Wen, and K.-F. Ma (2005). Frequency-dependent sites amplifications evaluated from well-logging data in central Taiwan, *Geophys. Res. Lett.* **32,** L21302, doi 10.1029/2005GL23527.

Hung, J.-H., Y.-H. Wu, and E.-C. Yeh (2005). Deformation and physical properties in the well of Taiwan Chelungpu fault drilling project, Takeng, west-central Taiwan, in *Asia Oceania Geosciences Society 2nd Annual Meeting*, 148 pp.

Jiang, S.-C. (1976). Seismic exploration in the Ilan plain, *Mining Technol.*, **14,** 215–221 (in Chinese).

Joyner, W. B., R. E. Warrick, and T. E. Fumal (1981). The effect of Quaternary alluvium on strong ground motion in the Coyote Lake, California, earthquake of 1979, *Bull. Seism. Soc. Am.* **71,** 1333–1349.

Klimis, N. S., B. N. Margaris, and P. K. Koliopoulos (1999). Site-dependent amplification functions and response spectra in Greece, *J. Earthquake Eng.* **3,** no. 2, 237–270.

Lee, C.-T., C.-T. Cheng, C.-W. Liao, and Y.-B. Tsai (2001). Site classification of Taiwan free-field strong-motion stations, *Bull. Seism. Soc. Am.* **91,** 1283–1297.

Lermo, J., and F. J. Chávez-García (1993). Site effect evaluation using spectral ratios with only one station, *Bull. Seism. Soc. Am.* **83,** 1574–1594.

Ma, K.-F., J.-H. Wang, and D. Zhao (1996). Three-dimensional seismic velocity structure of the crust and uppmost mantle beneath Taiwan, *J. Phys. Earth.* **44,** 85–105.

Malagnini, L. K., L. K. Mayeda, A. Akinci, and P. L. Bragato (2004). Estimating absolute site effects, *Bull. Seism. Soc. Am.* **94,** 576–590.

Ogura, K. (1988). Expansion of applicability for suspensor P-S logging, *Technical Report* No. 10, OYO Co., Japan.

Papageourgiou, A. S. (1988). On two characteristic frequencies of accel-

eration spectra: patch corner frequency and f_{max}, *Bull. Seism. Soc. Am.* **78,** no. 2, 509–529.

Satoh, T., H. Kawase, T. Iwata, S. Higashi, T. Sato, K. Irikura, and H. C. Huang (2001). S-wave velocity structure of the Taichung basin, Taiwan, estimated from array and single-station records of microtremors, *Bull. Seism. Soc. Am.* **91,** no. 5, 1255–1266.

Shieh, C.-F. (1992). Estimation of Q value by SP/S spectral ratio, *Terr. Atmos. Ocean. Sci.* **3,** 469–482.

Sokolov, V. Yu., C.-H. Loh, and K.-L. Wen (2004). Evaluation of generalized site response functions for typical soil classes (B, C, and D) in Taiwan, *Earthquake Spectra* **20,** 1279–1316.

Tanaka, H., C.-Y. Wang, W.-M. Chen, A. Sakaguchi, K. Ujiie, H. Ito, and M. Ando (2002). Initial science report of shallow drilling penetrating into the Chelungpu Fault zone, Taiwan, *Terr. Atmos. Ocean. Sci.* **13,** 227–251.

Zhang, F. (2004). Site response and attenuation analysis using strong motion and short-period data, *Ph.D. Dissertation*, Dept. Civil Struct. Environ. Eng., SUNY-Buffalo, 278 pp.

Graduate Institute of Geophysics
National Central University
Jung-Li, Taiwan 320
(M.-W.H., K.-F.M., C.-Y.W., J.-H.H., K.-L.W.)

Institute of Earth Sciences, Academia Sinica
P.O. Box 1-55
Nangang, Taipei, Taiwan 115
(M.-W.H., J.-H.W)

National Center for Research on Earthquake Engineering
Taipei, Taiwan 106
(K.-L.W.)

Manuscript received 26 June 2006.